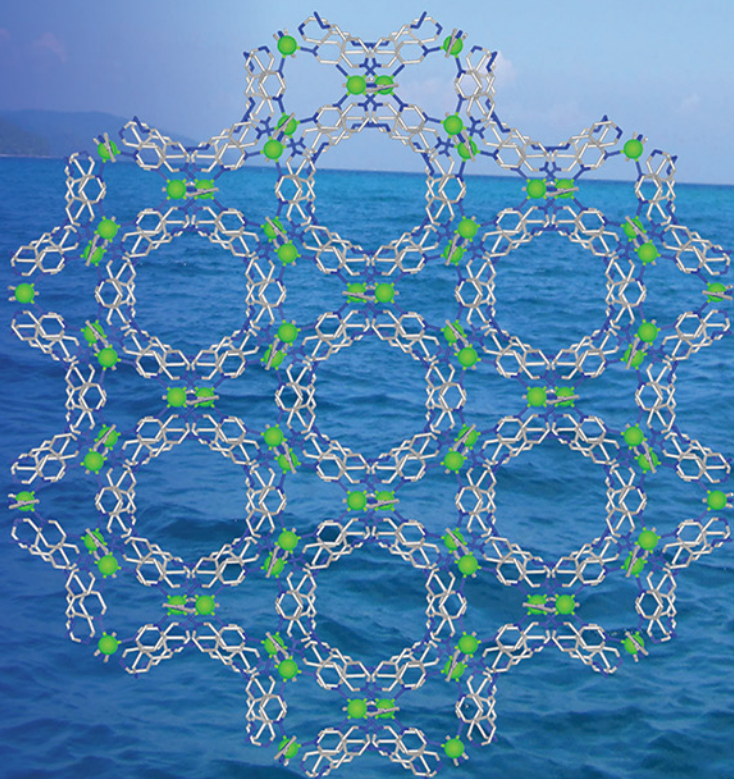# METAL-ORGANIC FRAMEWORKS (MOFs) FOR ENVIRONMENTAL APPLICATIONS

Edited by

SUJIT K. GHOSH

Sensing and sequestration of inorganic cationic pollutants by metal-organic frameworks

3

Zachary Lawrence Magnuson and Shengqian Ma*
Department of Chemistry, University of South Florida, Tampa, FL, United States
*Corresponding author: e-mail address: sqma@usf.edu

3.1   Cationic inorganic pollutants

Each section of this chapter includes a short synopsis of the cationic inorganic pollutant being addressed in the research discussed. Importantly, these introductions contain information on the speciation of the pollutant in relevant environmental compartments as well as the health effects and hazards they pose, particularly to humankind. Cationic inorganic pollutants consist of heavy metals and their oxidation products that are exotic and injurious to the environment and exhibit a tendency to exist in a cationic state. These compounds, which originate from the waste and/or end-product of industrial processes, can and should be remediated due to the negative effects they have. In most cases, alternative materials have been developed that are phasing out the need for products from these negligent industrial operations.

The materials discussed herein include cadmium, chromium, lead, mercury, and the nuclear waste products uranium, barium, cesium, and rubidium.

3.2   Design of metal clusters and organic linkers

The ability of metal-organic frameworks (MOFs) to selectively sense and sequester cationic inorganic pollutants depends on the careful selection of both of its components—the metal cluster and the organic linker. While the latter is most frequently functionalized, as we will see they each are capable of being controlled to serve some desirable purpose. The adsorption of cationic species to MOF structures is addressed by several key concepts. Firstly, the physical quality of the porous materials can be tailored with functional groups to draw the pollutant from the solution and localize it at the MOF in equilibrium with the rest of the solution [1]. The availability of these functional sites depends on their orientation in the crystal structure as well as the pore size and shape. Ideally, the functional part of linking ligands and metal clusters will point outward into the pore void, allowing for effective

interaction with the adsorbate, while the size of the pore can be tuned as a sieve, preventing atoms or molecules of certain size or shape (that may otherwise compete with the desired adsorbate) from entering the MOF. Secondly, the MOF can be designed to produce an electrostatic or Lewis acid−base interaction between its components and the cationic pollutant. A functional group amended to the MOF such as a thiol, sulfone, amine, or azine among others [2,3] can be utilized as a Lewis base to interact with the Lewis acidic cation, binding them together at the MOF's surface or within its porous interior directly. These binding sites can be occupied by guest ions that are less favorable than the pollutant, allowing for a controlled ion-exchange mechanism. Conditions for ion exchange can be optimized by consideration of hard−soft acid−base interactions, choice of nascent guest ion, ion concentration, and pH. Hydrogen bonding is also frequently considered and found to be the cause of effective adsorption.

3.3 Detection

High fidelity detection of cationic inorganic pollutants without employing destructive techniques can be designed in MOFs by considering the effects saturation with a desired analyte will have on how the clusters or ligands behave. This can manifest itself as changes in color, vibrational energies, electronic transitions, conductivity, luminescence quenching, and secondary or even tertiary interactions with concomitant compounds [4,5]. These methodologies will be highlighted in each section as they are employed in the work discussed. The changes that occur in the material can be analyzed using techniques such as Fourier-transform IR (FT-IR), X-ray photoelectron spectroscopy (XPS), UV-Vis diffuse reflectance, or even chronoamperometric measurements, among others; these data can then be correlated to the known concentration of analyte in a solution and used to determine unknown concentrations in real samples.

3.4 Selectivity

An effective sensor or remediator should also be able to target an analyte with high specificity and measure content accurately, ideally in the presence of multiple contaminants. Careful tuning using the concepts just mentioned enables this and testing is performed using detection analysis methods coupled with several types of studies, which likewise are highlighted in the research being reviewed. An example method would be parallel testing, where the MOF is exposed to individual competitive ion solutions to show results for each, followed by addition of the analyte to show a change in results. This technique and variations of these kinds of studies are common for characterization of MOFs, as are the ever-important real-world sample studies!

3.5 Cadmium

The element cadmium was discovered simultaneously as an impurity in zinc carbonate, also known as calamine, by Freidrich Stromeyer and Karl Leberecht Hermann in 1817. Its name is taken from the Latin word *cadmia*, for the mineral it was found in. Much like its periodic neighbors zinc and mercury, cadmium is most commonly found in a $+2$ oxidation state. The group 12 metal does not have partly filled *d* or *f* electron shells making it unlike most other transition metals in terms of reactivity and electronic behavior. Its most common uses in alloying, electroplating, and battery manufacture have fallen to the wayside as less toxic alternatives have been discovered.

3.5.1 Health and hazards

Cadmium is present in human diet as an oxide, having the highest known concentration in shellfish, seeds, and grains. These foodstuffs, among others, most effectively accumulate the metal from their environment [6]. Dietary intake is minor compared to routes involving gaseous or colloidal inhalation, which occur in occupational settings where the metal is processed and in cigarette smoke. These routes can result in lung cancer [7] among other kinds [8], as well as renal diseases and osteoporosis. Multiple regulatory agencies across the world have deemed cadmium a carcinogen.

3.5.2 Speciation

The IUPAC definition of speciation: "the distribution of an element amongst defined chemical species in a system" [9]. Speciation of the element being considered, in this section cadmium, is critical to understand how it will accumulate in various systems and determine the means of exposure. The natural occurrence of cadmium is scant, save for the zinc ores that are mined for it. Anthropogenic emissions present the main cause of cadmium pollution, resulting in particularly high concentrations around urban industrialized areas. Cadmium from industrial processes is often associated with chloride, resulting in highly soluble forms such as CdS, $CdSO_4$, $CdCl_2$, and Cd-aluminosilicates. In aqueous solution these compounds yield Cd(II) to some extent which is the form the MOFs reviewed here interact with.

3.5.3 Calcium-based metal-organic framework FJI-H9 [10]

Hui Xue, Maochun Hung, et al. had work published in Chemical Science in 2016 regarding the reversible uptake of Cd(II) in a regenerative MOF and characterized the materials' ability to both adsorb the metal and provide a means for in situ detection down to 10 ppm. Taking inspiration from work done for the adsorption of Hg (II) by strong Hg-S interactions [11], MOF FJI-H9 achieves up to $286\,\mathrm{mg\,g^{-1}}$
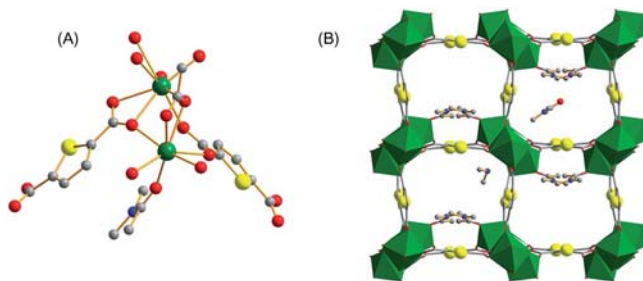
Figure 3.1 (A) Coordination environment of FJI-H9. Labeling follows C = gray, N = blue, O = red, S = yellow, Ca = green, and H is omitted. (B) Crystalline framework with Ca clusters as green polyhedra reveals pore shape and size, as well as functional group orientation.
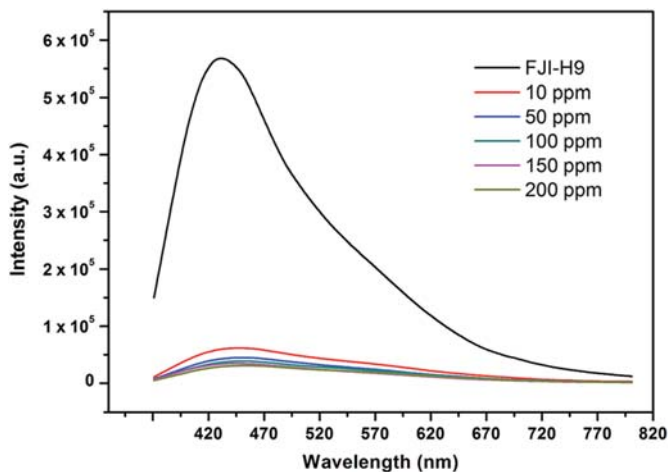*Source*: Adapted from H. Xue, Q. Chen, F. Jiang, D. Yuan, G. Lv, L. Liang, et al., A regenerative metal-organic framework for reversible uptake of Cd(ii): from effective adsorption to in situ detection, Chem. Sci. 7 (9) (2016) 5983−5988 with permission from The Royal Society of Chemistry.

adsorption of Cd(II) ions. The MOF is generated by the reaction of 2,5-thiophenedi-carboxylate with $CaCl_2$, forming an orthorhombic crystal of structure $[Me_2NH_2{}^+]$ $[Ca_2(C_6H_2O_4S^{-2})_2(CH_3COO^-)(DMA)]$•DMA (dimethylacetamide) (Fig. 3.1).

Crystals of FJI-H9 were soaked in 0.1 M cadmium nitrate/acetonitrile solution. The cadmium loaded MOF was washed with acetonitrile and characterized by several combustion analysis techniques—carbon/hydrogen/nitrogen analysis (CHN) and inductively coupled plasma (ICP), as well as elemental and thermogravimetry-mass spectrometry (TG-MS). The latter revealed a 2.5:1 cadmium to calcium ratio and TG-MS showed 15.5% composition of volatile solvents. These data led the group to report that 1 mol of the MOF was able to sequester 1.78 mol of Cd(II). The material moderately adsorbs mercury, but is otherwise selective.

Extended X-ray absorption fine structure (EXAFS) suggests unexpectedly that there is no CdS interaction, but rather three variants of Cd-O interactions and the presence of four waters for every cadmium. This belies the presence of $Cd(H_2O)_4^{+2}$, possibly stabilized by closely held nitrate anions. Based on IR signal differences, the group posits that Cd(II) ions displace the methylammonium ions in the framework, providing more favorable counterion stability. FJI-H9 was shown to effectively indicate the presence of cadmium ions at low concentrations via a fluorescence quenching mechanism. Fig. 3.2 shows several concentrations of aqueous cadmium nitrate and the respective change in emission intensity.

The group believes this is a product of Cd(II)-DMA (dimethylacetamide) interaction. Under the same conditions, this quenching is not observed for other heavy metals such Mg(II), Co(II), Ni(II), Mn(II), Zn(II), Fe(II), and Pb(II), and importantly, Hg(II), which is the only other heavy metal tested to have substantial adsorption. Importantly, the framework can be in situ deconstructed and subsequently regenerated with a 10% loss of material each cycle.

Figure 3.2 Fluorescence emission spectra for FJI-H9 in several Cd solution concentrations illustrating quenching effect.
Source: Adapted from H. Xue, Q. Chen, F. Jiang, D. Yuan, G. Lv, L. Liang, et al., A regenerative metal-organic framework for reversible uptake of Cd(ii): from effective adsorption to in situ detection, Chem. Sci. 7 (9) (2016) 5983–5988 with permission from The Royal Society of Chemistry.

3.5.4 Copper-based metal-organic framework utilizing sulfonic acid moieties [12]

Yang Wang, Guiqin Ye, et al. had work published in the *Journal of Materials Chemistry A* by the Royal Society of Chemistry in 2015 regarding a copper-based MOF that was stepwise postsynthetically modified with sulfonic acid groups for the selective uptake of cadmium from aqueous solutions. The MOF $Cu_3(BTC)_2SO_3H$ (BTC = 1,3,5-benzenetricarboxylate) or Cu-MOF for short was hydrothermally synthesized as $Cu_3(BTC)_2$ and then postsynthetically amended with thiol pendants at the metal Cu metal clusters. These were then oxidized to sulfonic acids, and each compound in the series was characterized to illustrate the enhancement of cadmium uptake. Successful attachment of the sulfonic acid group was confirmed by FT-IR which revealed S-O stretch bands from 1000–1350 wavenumbers. Structural integrity was considered by PXRD: $Cu_3(BTC)_2$ and Cu-MOF spectra were compared and found to be consistent. Spectra were also collected after the uptake of Cd(II) to further indicate structural steadfastness (Fig. 3.3). The BET surface area taken from N_2 adsorption isotherms at 77K of Cu-MOF was found to be 445 $m^2\,g^{-1}$, suggesting effective inclusion of the sulfonic acid groups as this is less than that of the unmodified $Cu_3(BTC)_2$.

Adsorption of Cd(II) was optimized to a pH of 6 and an exposure time of 10 minutes. At pH below 2.1 the sulfonic acid groups bear positive charge and repel Cd(II), while above pH 6 Cd(II) tends to precipitate as a hydroxide salt. Kinetic studies relying on the Lagergren pseudo-second-order kinetic model [13] revealed a
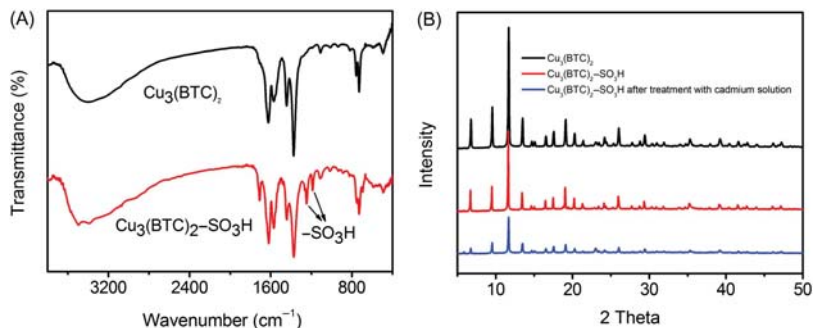
Figure 3.3 (A) FT-IR spectra showing introduction of sulfonic acid groups. (B) PXRD of $Cu_3(BTC)_2$, $Cu_3(BTC)_2$-SO$_3$H, and $Cu_3(BTC)_2$-SO$_3$H after treatment with Cd confirming structural integrity of Cu-MOF.
Source: Adapted from Y. Wang, G. Ye, H. Chen, X. Hu, Z. Niu, S. Ma, Functionalized metal-organic framework as a new platform for efficient and selective removal of cadmium (ii) from aqueous solution, J. Mater. Chem. A. 3 (29) (2015) 15292−15298 with permission from The Royal Society of Chemistry.

rate constant of 0.6818 g mg^{-1} min and the Langmuir model [14] (for monolayer adsorption) determined the maximum uptake capacity of 88.7 mg g^{-1}, conferring an ideal aging time. The adsorption was also characterized by the Freundlich model (for heterogeneous adsorption). The correlation coefficients (R^2) for each test point to the Langmuir model as a superior fit to the data collected, informing its use in determining the maximum uptake capacity. Further, adsorption isotherms were also taken for $Cu_3(BTC)_2$ and $Cu_3(BTC)_2$SH to illustrate the enhanced uptake of Cu-MOF by the careful postsynthetic modifications, reporting an uptake capacity of 67.8 and 74.5 mg g^{-1}, respectively. The ability for the unmodified parent structure to show adsorption of cadmium is attributed to complexation with residual carboxylate groups.

Selectivity against competing ions was characterized by parallel metal ion solutions of Na(I), Mg(II), Ca(II), Pb(II), Cu(II), and Ni(II) at concentrations ranging from 0.5 to 100 mg L^{-1} (with 1 mg L^{-1} Cd(II)). Cu-MOF retained a removal efficiency of at least 95.1% with Pb(II) being the strongest competitor. Desorption of Cd(II) from Cu-MOF was easily achieved by rinsing the laden material with deionized water and after oven drying could be reused. The material experienced a 15% decrease in adsorption capacity after six cycles and preservation of the crystalline structure was confirmed by PXRD, making it practical for recycled use.

3.6 Chromium

The lustrous, corrosion-resistant transition metal chromium was discovered in in 1797 by a French pharmacist while working with the lead mineral crocoite. The bronze swords and arrowheads found on soldiers of the Qin dynasty Terracotta

Army from the late 300s BCE were found remarkably well preserved due to a coating of a chromium oxide [15], illustrating the element's resistance to corrosion through its passivation by a dense, impermeable oxidized layer. This quality constitutes 85% of its commercial use as an electroplating metal and in the production of stainless steel [16]. Other important uses are in dying and pigmentation as a vivid red or yellow color, like that often associated with American school buses, though use of the lead-containing chromate (and other antiquated metal-based pigments) has declined with the advent of organic pigments.

3.6.1   Health and hazards

The two important forms of chromium when considering both the environment and human health are of the trivalent and hexavalent oxidation states. Cr(III) is an essential trace nutrient for mammals while Cr(VI) is a genotoxic carcinogen. In the environment, these two species transmute between one another depending on various conditions such as pH or the presence of tightly binding ligands [17]. Most chromium-containing ore is processed through Cr(VI) to sodium dichromate dihydrate, from which virtually all materials and compounds are prepared. The prevalence of the hexavalent form in this way leads human exposure during processing and application. Individuals working with stainless steel welding, for example, can generate Cr(VI) particles that lead to lung carcinomas, asthma, and damage to nasal epithelia and skin.

3.6.2   Speciation and reactivity

Though Cr(III) is not considered toxic, it is nevertheless important to develop an understanding of how it exists in the environment due to its equilibrium relationship with Cr(VI). In the unlikely absence of molecules with which it can form complexes (when considering natural waters), trivalent chromium in neutral or alkaline water primarily exists as $Cr(H_2O)_3$ and $CrOH^{2+}$. Cr(III) is a hard, acidic molecule that often forms hexacoordinate octahedral complexes with oxygen, nitrogen, and sulfur electron donors. Oxidation of Cr(III) to Cr(VI) in natural waters is generally low due to the high redox potential between the two species. It is reported [18] that the primary pathway involved mediation by manganese oxide. The presence and formation of Cr(VI) species hinges on both pH and concentration of Cr(VI). Within natural waters, CrO_4^{2+}, $HCrO_4^-$, and CrO_7^{2-} are prevailing species where the latter begins to condense to an orange-red dichromate ion above 10^{-2} M. Concentrations of chromium in freshwater range from 0.5 to 100 nM, while saltwater varies from 0.1 to 16 nM.

Speciation of chromium in terrestrial compartments likewise depends on pH—in acidic soils insoluble $Cr(OH)_3$ aq. dominates, but above pH 5.5 mainly $CrOH^{2+}$ is present. Regardless, both forms are strongly adsorbed by clay compounds or complexed by organic macromolecules such as humic acids which immobilize the metal. There are however complexing agents in soil, citric acid, for example, that enhance the solubility and mobility of chromium. Atmospheric chromium exists as

particles or droplets and serves as the main means of transport for the metal, with species following the same trends as those found in water, with a similar dependence of pH.

3.6.3 Cadmium metal-organic framework for Cr(VI) sensing and sorption [19]

Hung Fu, Ying Zhao, et al. had a manuscript accepted by Dalton Transactions in 2017 regarding the synthesis and characterization of a two-dimensional water stable MOF with high ethane and methane selectivity as well as efficient sensing and sorption of hexavalent chromium. The cadmium-based TIPA-MOF [Cd $(TIPA)_2(ClO_4)_2] \cdot (DMF)_3(H_2O)_2$ is constructed of triisopropanolamine (TIPA) linkages and contains perchlorate ions that exchange with Cr(VI). Crystals were characterized by single-crystal X-ray, PXRD, elemental analysis, and IR. The sensing capabilities of this MOF were investigated via parallel aqueous phase fluorescence emission tests of several compounds (BF_4^-, VO_4^{3-}, MoO_4^{2-}, WO_4^{2-}, ClO_4^-, SO_4^{2-}, NO^{3-}, Br^-, Cl^-, I^-, SCN^-, $Cr_2O_7^{2-}$, CH_3COO^-, OAc^-, $C_2O_4^{2-}$, OX^{2-}) at 0.0001 M concentration and 320 nm excitation wavelength. The dichromate ion was found to have the most significant quenching effect of the battery, the others being negligible (Fig. 3.4).

A solution containing potassium dichromate and concomitant ions at 10-fold greater concentration illustrated selectivity of the MOF for chromium as the quenching remained nearly the same as the equivalent solution of just dichromate. Titration experiments revealed an upper limit of 40 ppm and a lower limit of detection at 8 ppb. This is much lower than that of the contamination threshold of 100 ppb set by the US Environmental Protection Agency (EPA). Based on UV-Vis studies, the group proposes that the dichromate ions compete with the ligand for
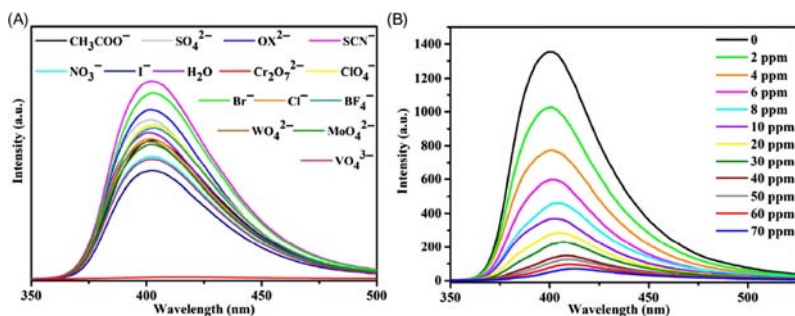
Figure 3.4 (A) Luminescence intensity spectra of TIPA-MOF in various anion solutions. (B) Emission spectra of TIPA-MOF in $K_2Cr_2O_7$ solutions at various concentrations.
*Source*: Adapted from H.-R. Fu, Y. Zhao, Z. Zhou, X.-G. Yang, L.-F. Ma, Neutral ligand TIPA-based two 2D metal-organic frameworks: ultrahigh selectivity of C_2H_2/CH_4 and efficient sensing and sorption of Cr(vi), Dalton Transact. 47 (11) (2018) 3725−3732 with permission from The Royal Society of Chemistry.

light absorbance, which would reduce ligand−metal charge-transfer ergo reducing luminescence. It is worth noting that PXRD revealed that quenching is not dependent on failure of the crystal structure, and in fact the material is reusable with 81% efficacy after five recycles. Adsorption of Cr(VI) was determined to be 116 mg g^{-1} at a 51% exchange with perchlorate ions after 24 hours.

3.6.4 Zirconium metal-organic framework MOR-2 high Cr(VI) adsorption [20]

Sofia Rapti, Debajit Sarma, et al. had a paper published by the Royal Society of Chemistry in the *Journal of Materials Chemistry A* in 2017 regarding a microporous MOF MOR-2 that can rapidly adsorb Cr(VI) with high capacity and be effectively adapted for use in ion-exchange chromatography.

The zirconium-based MOF ($H_{16}[Zr_6O_{16}(H_2PATP)_4] Cl_8 \cdot xH_2O$, $x = 8-12$) contains ((pyridin-1-ium-2-ylmethyl)ammonio)terephthalate (H_2PATP) ligands which, notably, are the first example of presynthetic amending of the terephthalate moiety with the large ammonium-pyridinium structure illustrated (Fig. 3.5). Typically, large functional substituents such as this adversely affect the growth of MOF crystals [21]. The chloride ions present serve to interchange with Cr(VI). MOR-2 crystal structure was characterized by PXRD, elemental analyses, thermogravimetric analysis, and energy-dispersive X-ray spectroscopy (EDS). It was found to have a BET surface area of 354 m^2 g^{-1} and type-I adsorption−desorption isotherms (suggesting microporosity) and ion-exchange experiments fitted to the Langmuir model report a maximum sorption capacity of Cr(VI) at 193.7 ± 6.7 mg g^{-1}, the highest reported when this work was published. Saturation of the compound with dichromate ion was reached within 1 minute with 99.1% removal capacity between pH of 2 and 9.
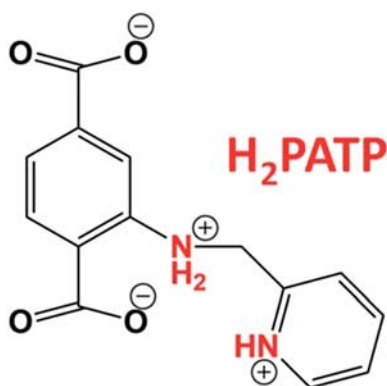
Figure 3.5 Illustration of the ligand H_2PATP highlighting functional sites.
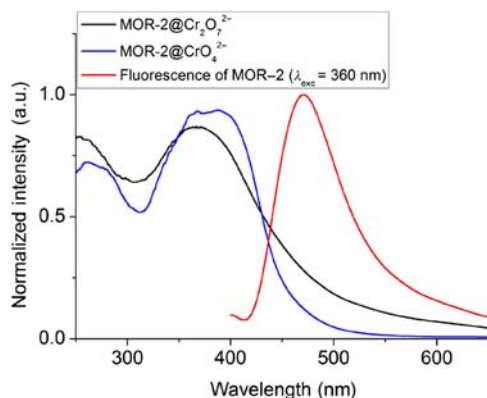*Source*: Adapted from S. Rapti, D. Sarma, S.A. Diamantis, E. Skliri, G.S. Armatas, A.C. Tsipis, et al., All in one porous material: exceptional sorption and selective sensing of hexavalent chromium by using a Zr^{4+} MOF, J. Mater. Chem. A 5 (28) (2017) 14707−14719 with permission from The Royal Society of Chemistry.

The ion-exchange column edition exhibits excellent functionality when compared to similar materials. MOR-2-HA was designed for use as a stationary phase, formed by suspension of MOR-2 in sodium alginate with the addition of HCl. This composite with the polysaccharide was necessary to prevent elution of MOR-2 in aqueous media, under which conditions it forms a viscous gum. Some characterization of MOR-2-HA is tabulated and additional information including ion-exchange column tests are reported.

Photophysical properties were determined using UV-Vis diffuse reflectance and steady-state emission spectroscopy. The former of MOR-2 shows absorption around 266 nm and a lower energy band from 380 to 450 nm. These bands belong to $\pi-\pi^*$ and $n-\pi^*$ transitions (n being the lone pair of the methylammonium group). The higher energy band at 266 nm sees contribution from Zr cluster transitions [22].

In the presence of chromate and dichromate, additional and unique features are observed that reflect ligand to metal charge transfer (LMCT) as illustrated in Fig. 3.6. Fluorescence titration experiments were performed to collect calibration curve data. A limit of detection (LOD) and limit of quantification (LOQ) were found to be 4 and 13 ppb, respectively. Using real samples of chrome plating waste in distilled water an LOD of 6 and LOQ of 18 ppb were found. When potable water was used instead, these values increased dramatically to 35 and 110 ppb.

The selectivity of MOR-2 was characterized by parallel tests against competitive ions for Cr(VI) ion exchange. Chloride, nitrate, and bromide ions had negligible effect even at 1000-fold concentration, but sulfate ions were able to lower the adsorptive capacity of MOR-2 to 52% at two- to fourfold concentration. Potable and industrial water samples containing varying amounts of these ions were able to be effectively remediated of Cr(VI) by MOR-2 as well, showing similar

Figure 3.6 Diffuse reflectance spectra for MOR-2 adsorbed with chromate and dichromate against fluorescence spectra revealing some overlap.
Source: Adapted from S. Rapti, D. Sarma, S.A. Diamantis, E. Skliri, G.S. Armatas, A.C. Tsipis, et al., All in one porous material: exceptional sorption and selective sensing of hexavalent chromium by using a Zr^{4+} MOF, J. Mater. Chem. A 5 (28) (2017) 14707−14719 with permission from The Royal Society of Chemistry.

fluorescence quenching resolution from 0 to 648 ppb. The mechanism proposed following density functional theory (DFT) calculations using $[PhNH_2CH_2\text{-}PyH]^{2+}$ as a model for H_2PATP suggested weak association of dichromate via three hydrogen bond interactions. Furthermore, chromate anions appear capable of deprotonating either the pyridinium or methylammonium ions, resulting in $HCrO_4^-$ ions that likewise associate with the ligand via hydrogen bonding.

3.7 Lead

The soft, ductile carbon homolog lead has the highest atomic number of any stable element and three of its isotopes are the products of the naturally occurring radioactive decay chains. It is easily isolable, ancillary to silver ore processing, and was first known by prehistoric western Asian people. Its inertness, ductility, and other physical qualities led to its widespread use which peaked in ancient Rome as plumbing (derivative of its Latin name *plumbum*), currency, roofing, and munitions. It has been proposed that the advent of lead plumbing played a part in the fall of Rome, though arguments against this are asserted based on its passivation in moist air or aerated water [23]. Nevertheless, lead is highly poisonous and affects nearly every organ in the body. Its wide array of modern uses, particularly in paint and fuels, has been greatly diminished with the advent of less toxic alternatives.

3.7.1 Health and hazards

Unlike most other toxic compounds or metals, there is no minimum acceptable exposure. Lead is primarily distributed to the brain, liver, kidney, and bones. Most of it is eventually excreted but some amount remains stored in bones and teeth. Children are particularly susceptible to lead poisoning as they absorb and retain three to five times the amount adults do [24]. Common routes of exposure include mining and smelting of lead-containing ores as well as manufacturing and recycling of lead-based products. Most of the lead used now comes from recycling. The effects of lead exposure range in severity, but even at blood concentration levels of $5\,\mu g\,dL^{-1}$ leads to changes in brain development that result in decreased intelligence quotients and antisocial behavior. It has also been linked to hypertension, anemia, immunotoxicity, and damage to reproductive organs. Organolead compounds are particularly dangerous as they are readily absorbed through the skin and lungs.

3.7.2 Speciation

Lead in nature commonly occurs in two oxidations states: Pb(IV) and Pb(II). The former is typical of lead's organic chemistry and common for the carbon group, while the latter is characteristic of its inorganic chemistry. The presence of organolead compounds in the environment is generally attributed to the use of alkylated species used as antiknocking agents in fuels. These tend to decompose to some extent but are highly bioavailable. Inorganic lead species are found as the free ion

and in other bound forms; the most common are PbBrCl and PbBrCl $\cdot$ $(NH_4)_2SO_4$ as products of vehicle exhaust and $Pb(SO_4)$ which is associated with lead smelting processes. The species of lead present in terrestrial samples is directly related to concentration and pH [25,26].

3.7.3   Lanthanide-based metal-organic framework for selective detection of Pb(II) [27]

Guanfeng Ji, Jingjuan Liu, et al. had work published by the Royal Society of Chemistry in the *Journal of Materials Chemistry A* in 2017 regarding highly sensitive and selective detection of Pb(II) using a 2D terbium MOF. Produced under hydrothermal conditions, Tb-MOF ([Tb(3,5-dicarboxyphenolate anion)(H_2O)_5]) crystal structure was determined using single-crystal X-ray. Luminescence was characterized in solid state and aqueous conditions revealing excitation at 334 nm, common to lanthanides [28]. Emission peaks for the f-f transitions of Tb(III) were found at 492, 546, 587, and 623 nm and have been attributed to the LMCT from the antennae-like effect of the ligand. The group also reports negligible change in luminescence intensity after storage in deionized water or across pH values of 3−12, adjusted used HCl and NaOH.

Selectivity capabilities were analyzed using parallel metal ion aqueous solutions to determine the quenching effects of various metals, as shown in Fig. 3.7. These
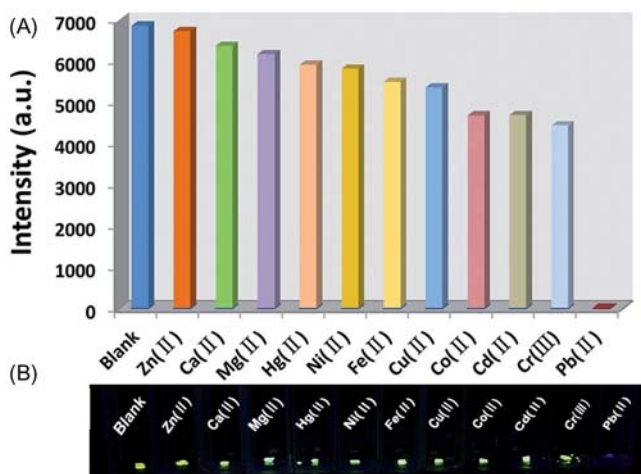
Figure 3.7 (A) Luminescence intensities of $^5D_4$-$^7F_5$ transitions [4] at 545 nm of Tb-MOF in 0.001 M metal ion solutions. (B) Images of Tb-MOF associated with each metal ion under UV light.
Source: Adapted from G. Ji, J. Liu, X. Gao, W. Sun, J. Wang, S. Zhao, et al., A luminescent lanthanide MOF for selectively and ultra-high sensitively detecting Pb^{2+} ions in aqueous solution, J. Mater. Chem. A 5 (21) (2017) 10200−10205 with permission from The Royal Society of Chemistry.

were prepared at 0.001 M and the results shown were determined after two hours. The quenching effect can be seen by the naked eye. Quantitative analysis of the quenching efficiency was characterized using a Stern−Volmer equation and suggest an excellent, nearly linear correlation coefficient at low concentrations (8×10^{-4} to 3.4×10^{-7} M, the lower concentration end being the LOD). At higher concentrations a meaningful deviation from linearity is reported; the group believes this to be due to self-absorption by the metal ions. Selectivity was characterized similarly, but the battery of solutions was replaced with a concomitant solution of previous metal ions, where their total concentration was 0.001 M. Luminescence intensity in this mixed solution remained above 88% and introduction of Pb(II) effectively quenched this.

Some applications work was performed. A thin film of Tb-MOF was fabricated by a hot-pressing process containing 0.5 wt.% of Tb-MOF. This material was applied to strips which were placed in a similar mixed-ion solution as that used for selectivity testing. These strips successfully made the qualitative determination of the presence of Pb(II) against other metal ions and show a simple and practical application of Tb-MOF for such analyses.

The mechanism of the quenching is believed to be due to electrostatic interactions between Pb(II) and the Lewis basic phenolic oxygen of the ligand. Characterization was done following luminescence lifetime studies which point toward a dynamic and a static mechanism. It was found that the UV-Vis absorption of the metal ions does not overlap with the absorption and emission spectra which could suggest that interaction between the ligand and Pb(II) significantly hinders the LMCT to the Tb(III). XPS and FT-IR confirmed a weak interaction between phenolic oxygen and Pb(II).

3.7.4 Electrochemical DNA-functionalized porphyrinic metal-organic framework for Pb(II) sensing [29]

Lin Cui, Jie Wu, et al. had work published in Analytical Chemistry in 2015 regarding an efficient electrochemical sensor for the detection of Pb(II) using an Fe(III) based MOF (FeP-MOF) containing porphyrinic ligands functionalized with DNA that amplifies electrochemical signals in the presence of Pb(II) against other metal ions, yielding a LOD of 0.034 nM. The complex functionality of this material relies on the catalytic cleavage of GR-5 DNA strand by Pb(II) from gold nanoparticles (AuNPs); the remaining strand attached to FeP-MOF via embedded AuNPs then hybridizes with a hairpin probe (HP) that is immobilized to a carbon electrode as illustrated in Fig. 3.8. The porphyrinic ligand then catalyzes the oxidation of chromogenic 3,3′,5,5′-tetramethylbenzidine (TMB) by hydrogen peroxide which is followed by the electrochemical reduction of the oxidation product at the sensors surface. Measurements are then made using a chronoamperometric method that can be correlated to Pb(II) concentration as a significant increase in steady-state current.

The biomimetic oxidase-like catalytic properties of FeP-MOF were evaluated by reaction of TMB with H_2O_2 in aqueous solution. It was shown by current-voltage (CV) electrochemical measurement that modification of a carbon electrode with
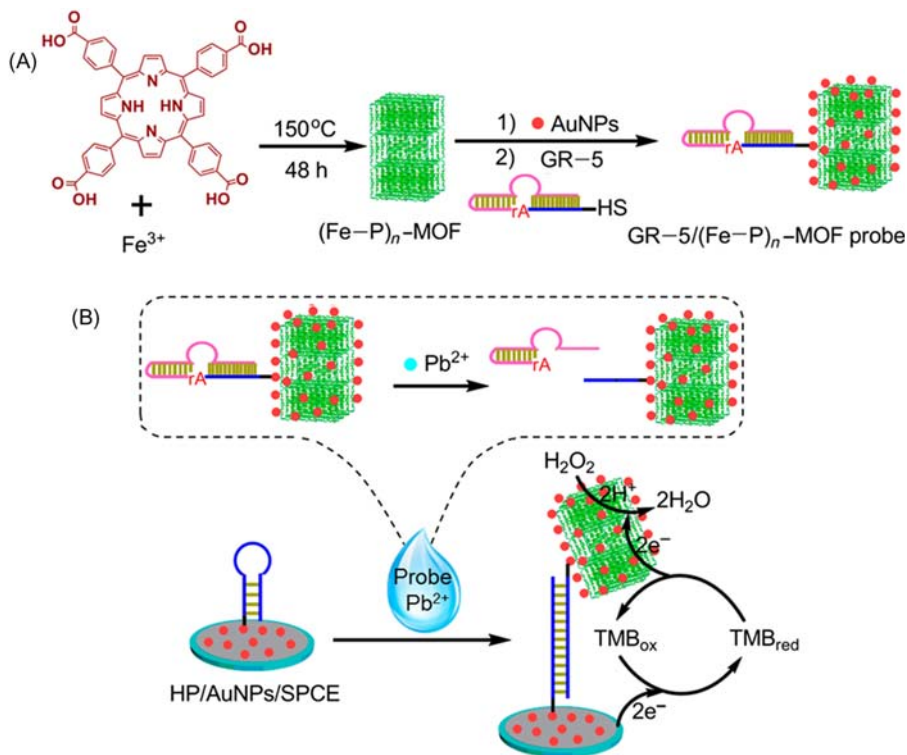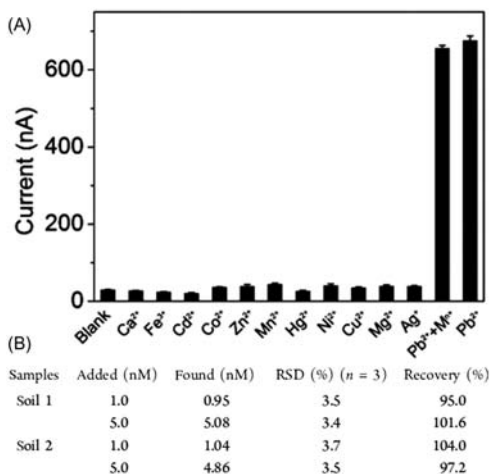
Figure 3.8 (A) FeP-MOF synthesis and functionalization with GR-5. (B) Ability of FeP-MOF to detect Pb(II) in solution and mimic peroxidase allowing it to interact with the cathode. *Source*: Adapted from L. Cui, J. Wu, J. Li, H. Ju, Electrochemical sensor for lead cation sensitized with a DNA functionalized porphyrinic metal-organic framework, Anal. Chem. 87 (20) (2015) 10635−10641 with permission from the American Chemical Society.

FeP-MOF increased the reduction peak current, indicative of an electrocatalytic reaction. Stability of this component of the material's functionality was determined. FeP-MOF-modified carbon electrodes were exposed to pH ranging from 3 to 10 and temperatures from 4°C to 60°C for 2 hours. At pH of 3 and 10, catalytic activity was found to be 62.3% and 41.9%, respectively. At 60°C it maintained 87% activity. This is impressive compared to biological counterparts horseradish peroxidase and hemin, which maintain activities of 1.3% and 18.6% at pH 3, and 11.6% and 20.8% at pH 10, respectively.

The structure of the MOF that FeP-MOF is amended from was used to confirm the crystal structure of FeP-OF by X-ray diffraction (XRD) [30]. The material has a BET surface area of 279 $m^2 g^{-1}$ and FT-IR was used to show metalation with Fe (III) of the porphyrinic ligand. Embedding of AuNPs to FeP-MOF was shown by an absorption peak of 520 nm that did not occur prior to inclusion as well as SEM imaging revealing dispersion across the surface.

(A)

(B)

Samples	Added (nM)	Found (nM)	RSD (%) ($n = 3$)	Recovery (%)
Soil 1	1.0	0.95	3.5	95.0
	5.0	5.08	3.4	101.6
Soil 2	1.0	1.04	3.7	104.0
	5.0	4.86	3.5	97.2

Figure 3.9 (A) Chronoamperometric response of FeP-MOF to 5 μM metal ion solutions at +100 mV. $Pb^{2+}M^{n+}$ data represents FeP-MOF in the presence of a mixed metal ion solution at same concentration. (B) Chart showing determination of Pb(II) in spiked soil samples. RSD is relative standard deviation.
Source: Adapted from L. Cui, J. Wu, J. Li, H. Ju, Electrochemical sensor for lead cation sensitized with a DNA functionalized porphyrinic metal-organic framework, Anal. Chem. 87 (20) (2015) 10635−10641 with permission from the American Chemical Society.

Sensitivity of the material to Pb(II) characterized under optimized conditions revealed an impressive correlation coefficient of 0.9994 ranging from 0.05 to 200 nm. The LOD of 0.034 nm is 350 times lower than that permitted in drinking water by WHO. Application of this material to real samples was done using spiked soil samples. Related data is tabulated in Fig. 3.9. Selectivity was investigated using a mixed metal ion solution. At 50-fold concentration of competing ions a negligible response was observed.

3.8 Mercury

The element mercury has been found in Egyptian tombs dating back past 1500 BCE. It has been known of and collected for various ritualistic and extravagant reasons for millennia. It was believed to be the *prima materia* (first material) of metal [31], from which all metals came, and possessed healing and life extending properties. Now, the heavy d-block element is known for its toxicity and modern usage in various measuring instrumentation such as thermometers and barometers. The application of mercury in these tools is being phased out as less harmful alternatives are found. Industrial uses of mercury, such as the production of sodium hydroxide and chlorine from salt, are also being replaced.

D	Dental problems and amalgam release of mercury
E	Endocrine toxicity and dysfunction
A	Affects adrenal function and hormone production (inhibiting of 21α-hydroxylase)
D	Diabetes may be associated or caused
L	Likely inhibits myelin synthesis in developing feti and children
Y	Young's syndrome (Azoospermia sinopulmonary infections)
M	Methylation of inorganic mercury in body
E	Environmental accumulation (soil, water, air)
T	Toxic to GI, liver, and pancreas
H	Hypertension due to epinephrine excess (inhibits catecholamine metabolism)
Y	Young women should avoid some fish
L	Long biological half-life (may be >90 days)
M	Microorganisms (sulfate processers) synthesize from inorganic mercury
E	Enters food chain, bio accumulates, and biomagnifies
R	Red blood cell accumulation (competes with iron for hemoglobin binding)
C	Crosses blood-brain barrier and produces central nervous system toxicity
U	Uterine fetal toxicity
R	Renal toxicity, especially to renal tubules
I	Immune, enzyme, and genetic alterations
A	Association with many neurodegenerative diseases
L	Long-term toxicity on many organs and systems
S	Special senses affected

Figure 3.10 Mnemonic for various health effects induced by mercury exposure.
Source: Developed by K.M. Rice, E.M. Walker, M. Wu, C. Gillette, E.R. Blough, Environmental mercury and its toxic effects, J. Prev. Med. Public Health 47 (2) (2014) 74−83 [33].

3.8.1   Health and hazards

Mercury is the third most toxic substance on the planet, ranked by the Agency for Toxic Substances and Disease Registry, coming after arsenic and lead. Exposure to humans has three main routes: pigments used in paints and plastics predating 1990; mercury vapors present in fossil fuels, medical waste incineration, and industrial processes; and finally through bioaccumulation. The latter occurs through bacteria that consume inorganic mercury compounds that they fix into organic methylmercury. This tends to reach its highest biological concentration in fish, which are then consumed by humans [32]. The average body half-life for MeHg is 40 days—in the brain it can be up to 20 years.

The slew of negative health effects and issues caused by various forms of mercury has been contained in the mnemonic DEADLY METHYLMERCURIALS (Fig. 3.10). Mercury exposure can result in more than 250 unique symptoms which can complicate diagnosis.

3.8.2   Speciation

About half of the mercury introduced to the environment comes from volcanic activity, the other half primarily from coal-fired power plants and gold production. Elemental and mercuric forms, Hg(0) and Hg(II) respectively, exist in the atmosphere in equal parts but the latter is the most important when considering exposure and reactivity. Hg(II) is generally associated with halogens such as $HgCl_2$ and hydroxide. These species are highly water soluble and, as an example, can be

absorbed in cloudwater where it would later be introduced to the ground or bodies of water as rain. In general, these common species of mercury undergo several transformations, interchanging with one another: Hg(0) can be oxidized to Hg(II) by ozone, hydroxyl radicals, or hydrogen peroxide (all present in air moisture); Hg (II) can be reduced to Hg(0) by reaction with gaseous sulfates or aqueous sulfites [34]. While atmospheric mercury can interact directly, the deposition into terrestrial and aquatic systems that leads to bioaccumulation in the foods we eat accounts for the greatest amount of exposure.

3.8.3 Postsynthetically modified UiO-66 for selective detection [35]

Xin Zhang, Tifeng Kia, et al. had work published in the *Journal of Solid State Chemistry* in 2017 regarding a zirconium-based MOF for the selective sensing of Hg(II) in aqueous medium. The group utilizes copper catalyzed click chemistry to postsynthetically modify UiO-66-N_3 with phenylacetylene, generating a triazole with which Hg(II) is expected to bind. The intense luminescent properties of this moiety are strongly quenched in the presence of mercury- readily differentiated from concomitant metals due to their lesser binding affinities. Experimental characterization of this follows like solutions (1 mL, $10 - 2$ M) of several cationic metals $M(NO_3)z$ ($Mz + = Ca^{2+}$, Al^{3+}, Cr^{3+}, Fe^{2+}, Fe^{3+}, Co^{2+}, Ni^{2+}, Cu^{2+}, Na^+, K^+, Mg^{2+}, Ag^+, Zn^{2+}, Hg^{2+}, and Pb^{2+}) (Fig. 3.11). Results suggest a high specificity
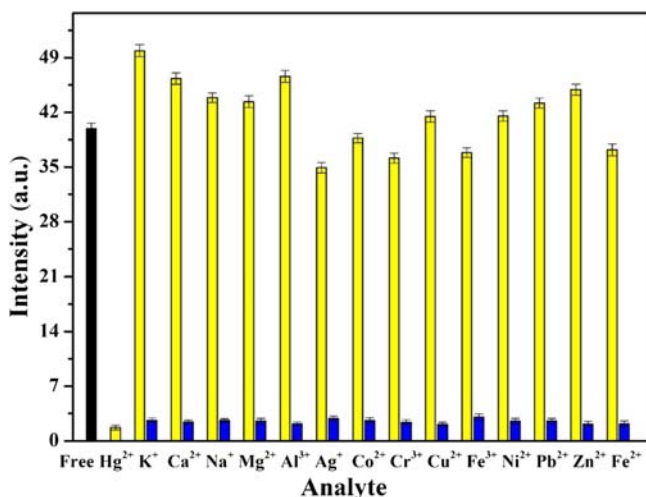

Figure 3.11 Black bar represents fluorescence of UIO-66-PSM at 544 nm. Yellow bars are 30 s after the addition of 10 mM of metal ion, while blue bars measure these solutions after the addition of Hg(II).
Source: Adapted from X. Zhang, T. Xia, K. Jiang, Y. Cui, Y. Yang, G. Qian, Highly sensitive and selective detection of mercury (II) based on a zirconium metal-organic framework in aqueous media, J. Solid State Chem. 253 (2017) 277−281 with permission from Elsevier.

for mercury which the group attributes to several factors: Hg(II)'s relatively larger radius, its diverse coordination, the rigidity and soft-acid character of the triazole moiety, and the strong Hg-N interaction.

The crystal structure of UiO-66-PSM was characterized with scanning electron microscopy, showing an octahedral geometry and nanoparticle size of $500-600$ nm, and powder X-ray diffraction, which yielded a pattern in good accordance with that of simulated UiO-66 [36]. FT-IR spectra of UiO-66-N_3 displayed one peak at 2120 wavenumbers, indicative of an azide asymmetric stretch. Following postsynthetic modification this peak is reduced, which is ascribed to the change from azide to triazole. for the N_2 sorption studies at 77K gave a BET surface area of 412.45 $m^2 g^{-1}$ for UiO-66-PSM. The postsynthetic transformation is further elucidated by excitation and emission studies. UiO-66-N_3 had very weak fluorescence due to the electron withdrawing azide, while UiO-66-PSM, upon excitation at 484 nm, produced a strong broad band emission around 544 nm from the $\pi-\pi^*$ transition of the organic linkers. The bonding of Hg(II) into the PSM MOF at the triazole is characterized by XPS. The N 1s peak at 403.4 eV is shifted to 406 eV upon the addition of mercury, showing N$-$Hg interaction that explains the quenching effect.

A linear relationship between fluorescence quenching and mercury concentration was established from 0 to 78.1 μM and indicates UiO-66-PSM can be used for quantitative determination of Hg(II) (Fig. 3.12). A limit of detection value of 5.88 μM is comparable to previously reported fluorescence sensors. A final test against real water samples with added mercury describe the practical application of the MOF.
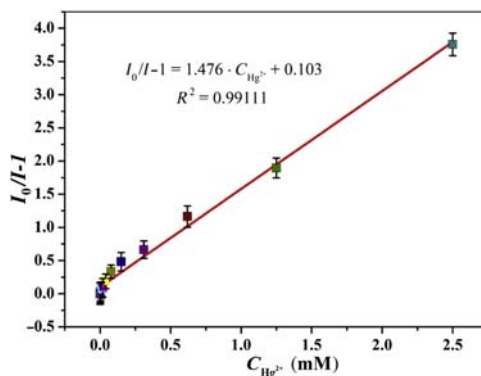

Figure 3.12 Stern$-$Volmer plot of $I_0/I-1$ versus the concentration of Hg(II), showing a good fit. Where I_0 and I are the luminescence intensities before and after Hg(II) inclusion. *Source*: Adapted from X. Zhang, T. Xia, K. Jiang, Y. Cui, Y. Yang, G. Qian, Highly sensitive and selective detection of mercury (II) based on a zirconium metal-organic framework in aqueous media, J. Solid State Chem. 253 (2017) 277$-$281 with permission from Elsevier.

3.8.4 *UiO-66-NH$_2$ DNA* [37]

Lan-Lan Wu, Zhuo Wang, et al. had work published in ChemPubSoc Europe in 2016 regarding the preparation of a MOF-DNA hybrid for the selective fluorescent-based sensing and sequestration of Hg(II), down to 17.6 nM concentration. The key to this material's functionality lies in the binding affinity of mercury ions to thymine−thymine (T-T) mismatched pairs in oligonucleotides. Mercury fits between the interacting faces of the base pairs, creating a thymine−Hg(II)−thymine sandwich complex (T-Hg^{2+}-T) [38]. The group incorporates a thymine rich single-stranded DNA (ssDNA) labeled with a fluorophore (FAM) at the 3' end to serve as a probe (Fig. 3.13).

The probe strongly fluoresces at 480 nm under 510 nm light. When in the presence of UiO-66-NH$_2$, photoinduced energy transfer (PET) quenches the probe via hydrogen interactions and π−π stacking between the aromatic organic linker and the base-pair groups of the dye. When Hg(II) is introduced, the formation of hairpin-like T-Hg(II)-T structures affect the conformation of the dye and isolate it from UiO-66-NH$_2$, restoring fluorescence. This suggests that the MOF-DNA system's fluorescence intensity is a function of mercury concentration. To characterize their theory, fluorescence emission spectra under varying conditions in a 7.4 pH tris-HCl buffer were collected. The free probe has strong emission at 510 nm which declines with the introduction of the modified UiO-66; the fluorescence quenching efficiency (Q_e) is found to be close to 75% (Fig. 3.14). Further, the introduction of Hg(II) significantly enhances the otherwise quenched signal, noting that the probe is not affected by just mercury—the presence of UiO-66-NH$_2$ is necessary. Inversely, the UV/Vis diffuse reflectance spectrum of UiO-66-NH$_2$ shows there is no absorbance from the material at the dyes emission wavelength, indicating fluorescence resonance energy transfer does not occur between the two.
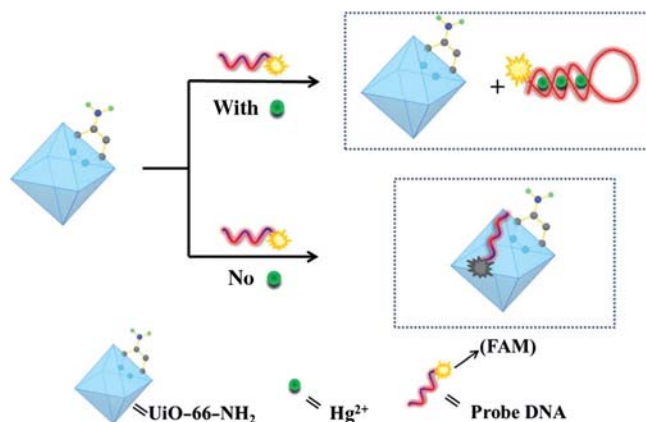
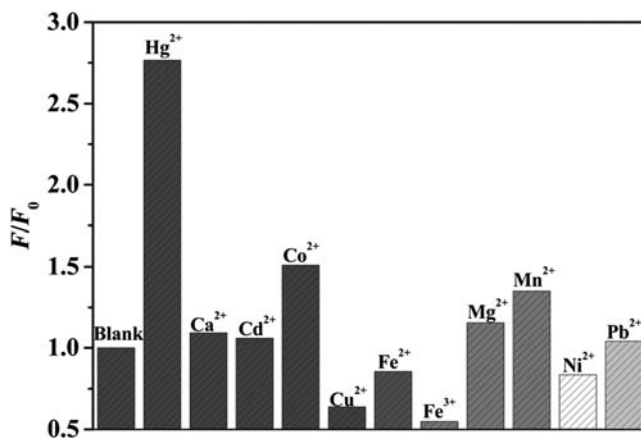**Figure 3.13** Conceptual illustration of the fluorescence mechanism.
Source: Adapted from V. Guillerm, S. Gross, C. Serre, T. Devic, M. Bauer, G. Ferey, A zirconium methacrylate oxocluster as precursor for the low-temperature synthesis of porous zirconium(iv) dicarboxylates, Chem. Commun. 46 (5) (2010) 767−769 with permission from the American Chemical Society.
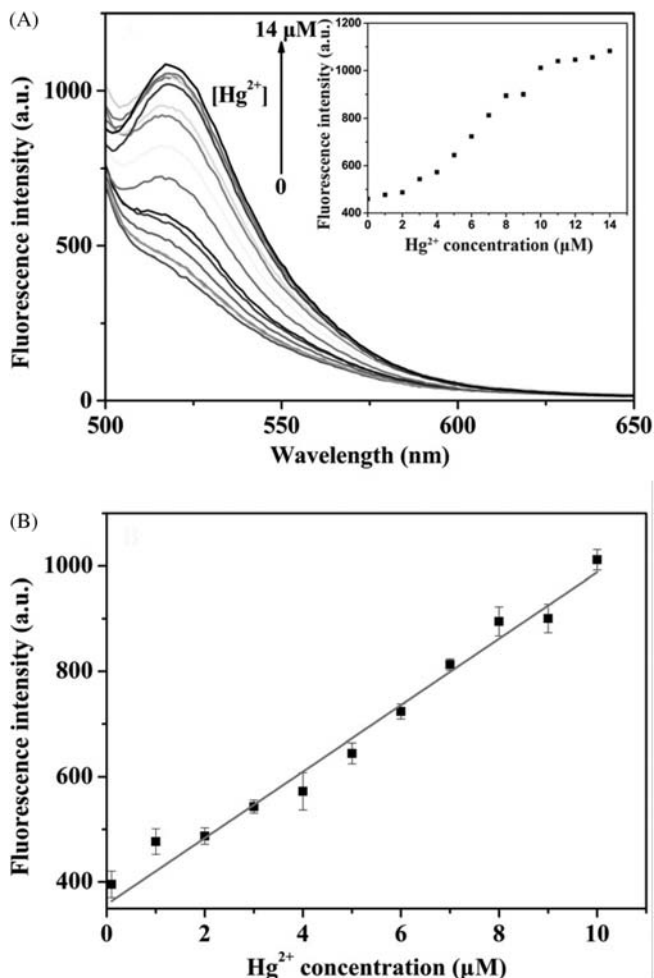
Figure 3.14 (A) illustrates the relationship between Hg(II) concentration and fluorescence intensity across 500−650 nm. Each fluorescence curve is representative of a point on the inset graph. (B) Expresses the linear relationship between fluorescence intensity and Hg(II) concentration.

Source: Adapted from X. Zhang, T. Xia, K. Jiang, Y. Cui, Y. Yang, G. Qian, Highly sensitive and selective detection of mercury (II) based on a zirconium metal-organic framework in aqueous media, J. Solid State Chem. 253 (2017) 277−281.

The selectivities for various metals were tested under identical conditions to that of the Hg(II) fluorescence tests. Fig. 3.15 illustrates the significant fluorescence enhancement relative to the other cationic metals tested. It is worth noting that the detection limit reported is lower than the toxicity level in drinking water (30 nM) for mercury as defined by the World Health Organization (WHO) (Fig. 3.16).

Figure 3.15 Selectivity of the MOF-DNA system against other metals. F_0 and F represent the fluorescence intensity before and after the addition of 10 μM metal ions, respectively.
Source: Adapted from V. Guillerm, S. Gross, C. Serre, T. Devic, M. Bauer, G. Ferey, A zirconium methacrylate oxocluster as precursor for the low-temperature synthesis of porous zirconium(iv) dicarboxylates, Chem. Commun. 46 (5) (2010) 767−769 with permission from the American Chemical Society.
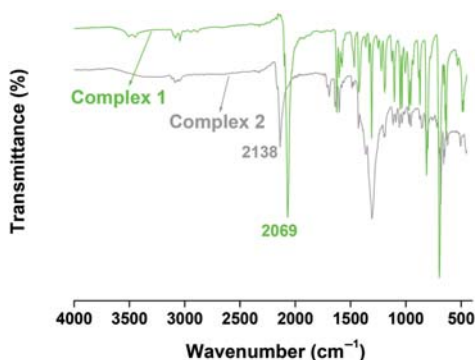
Figure 3.16 FT-IR spectra showing SCN-MOF (Complex 1) prior to inclusion of Hg(II) and after (Complex 2), illustrating the blueshift effect of the metal ion adsorption.
Source: Adapted from H. Urata, E. Yamaguchi, T. Funai, Y. Matsumura, W. Si, Incorporation of thymine nucleotides by DNA polymerases through T−HgII−T base pairing, Angew. Chem. 122 (37) (2010) 6666−6669 with permission from The Royal Society of Chemistry.

3.8.5 Nickel-based metal-organic framework for visual detection and selective remediation [39]

Shibashis Halder, John Mondal, et al. published work in the journal *Dalton Transactions* in 2017 regarding a MOF capable of remediation of Hg(II) ions from water with high selectivity for the cation and a visual indication of its presence.

Relying on the affinity of Hg(II) to coordinate with large, soft atoms such as sulfur [40], the group proposes a nickel-based MOF $[Ni(3-bpd)_2(NCS)_2]_n$, where 3-bpd is 1,4-bis(3-pyridyl)-2,3-diaza-1,3-butadiene, referred to as SCN-MOF. Analyses show that two thiocyanato moieties bind the Ni center with uncoordinated S, offering conditions for the binding of Hg(II). This is confirmed by FT-IR spectra where the typical 2069 wavenumbers band of SCN^- blueshifts in the presence of Hg(II) as CN bond order increases and electron density is pulled away from the sulfur.

Mercury uptake studies were performed by measuring change in color (from green to gray) of a Hg(II) and SCN-MOF solution over time, and efficiency was characterized by the amount of Hg(II) remaining in the solution after the uptake studies completed. Selectivity was characterized by a battery of tests against other metals and metalloids (Al^{3+}, Zn^{2+}, Fe^{3+}, Na^+, K^+, Mg^{2+}, Ca^{2+}, Pb^{2+}, Cd^{2+}, As^{3+}, and Ag^+) that relied on the observation of color change, all performed in aqueous solution under ambient conditions. No other metal tested elicited a visually appreciable change in color, suggesting little to no interaction through a similar mode as Hg(II). The insolubility of the MOF in aqueous solution provides a simple means of separation—filtration of the solid complex after Hg(II) uptake effectively remediates the water of its mercury content. The group suggests a 2:1 ratio of nickel to mercury in the Hg(II)·MOF complex by theoretical calculations, where two Hg(II) bond through one sulfur via S-Hg and weak Hg-Hg interaction. The possibility of transmetalation was explored by analysis of mother liquor for free nickel ions with dimethylglyoxime in ammoniacal medium, which was not positively confirmed by a telling red precipitate. The binding and removal process was found to be irreversible. Treatment of the Hg(II)·MOF complex with thiourea and hydrochloric acid precipitated mercuric sulfide but also resulted in the decomposition of the MOF.

3.9   Radioactive wastes

The waste generated from the manufacture and use of nuclear fuel is separated into three phases: the front end, when radioactive ore is processed into fissionable material; the service period, during which the fuel is being spent; and the back end, when the spent fuel is reprocessed into forms suitable for safe storage. On the front end of the process, uranium ore is located and mined using open-pit or leaching methods. The ore is milled into U_3O_8, also known as yellowcake, then converted either to UF_6 which is later enriched, or UO_2, depending on the kind of reactor it is meant for. The service period includes safe and reliable transport of fissile material and management of the active fuel rods. The back end considers methods for separation of remaining fissile material (for reuse) from spent fuel which is solution-based and increases the overall amount of waste but generally reduces its radioactivity [40]. There are multiple methods for this, but the most commonly employed is PUREX (Plutonium and Uranium Recovery by Extraction).

3.9.1   Health and hazards

Ionizing radiation can cause damage and abnormalities in living tissue. This is particularly dangerous with respect to DNA as changes to genetic material can result in cancer among other negative effects. Acute exposure to radiation can result in sickness or death within hours to days, while chronic exposure leads to delayed health issues such as cataracts, cancer, and benign tumors [41]. Routes of exposure are categorized and internal and direct. Internal exposure includes ingestion or inclusion of radioactive material into the body, where alpha and beta particles pose a serious threat to health. Direct exposure regards radiation from outside of the body. Alpha particles are too large to pass through clothing and skin, but beta and gamma radiation can penetrate the body.

3.9.2   Speciation

The constituents of radioactive waste considered here come from spent fuel rods. Materials that interact directly with the fuel rod such as cladding or fuel rod pools contain some amount of radioactive material as well and are also considered a waste product of nuclear reactors. Waste is classified as low-level (LLW), intermediate-level (ILW), and high-level (HLW). Spent fuel rods contain fission products of ^{235}U, primarily of which are ^{90}Sr and ^{137}Cs, but can include various other transuranic species, some of which are described in Fig. 3.17. Strontium is divalent and behaves similarly to calcium while Cesium is monovalent. Uranium has several common oxidation states (III, IV, and II) while plutonium has states I through IV.

3.9.3   Cryptand inspired metal-organic framework for detection and adsorption [42]

Sergey A. Sapchenko, Pavel A. Demakov, et al. had work published in *Chemistry: A European Journal* by ChemPubSoc Europe in 2017 regarding a zinc-based cryptand ligand MOF with luminescence dependent on the adsorption of group I metal cations. The material shows selectivity toward heavier alkali metals, Rb(I) and Cs

4.5%–7%	0.04%–1.25%	<0.001%
90-Sr	155-Eu	113-Cd
137-Cs and 135-Cs	85-Kr	121-Sn
99-Tc	151-Sm	
93-Zr	126-Sn	
	79-Se	
	107-Pd	
	129-I	

Figure 3.17 List of elements and their isotopes by percent content of the fission products of ^{235}U.

(I) in particular. $(H_3O)_2[Zn_4(ur)(Hfdc)_2(fdc)_4]$ (ur = urotropine, H_2fdc = furan-2,5-dicarboxylic acid) or C1 for short, was produced under solvothermal conditions and characterized using single-crystal X-ray revealing a 3D framework with 61% accessible volume containing two distinct pore types; one is hydrophobic and hosts DMF and water molecules, while the other has void-facing oxygens from the fdc^{2-} ligands with hydroxonium counterions. The latter pore is similar to the container-like cryptand supramolecules which strongly complex cationic guests by oxygen and nitrogen lone-pair interactions.

Adsorption of metal cations by C-MOF was characterized by soaking in 0.01 M metal nitrate solutions in NMP for 1 day. Crystal stability was confirmed by PXRD and metal content was determined by dissolution in H_2O_2/DMF followed by atomic emission spectroscopy (AES), revealing preferential binding for Rb(I) and Cs(I) over Li(I), Na(I), or K(I). Selectivity was characterized with a 0.001 M concomitant metal nitrate solution containing all five metals referred to previously. It was found that less than 10% of hydroxonium cations were replaced by Li(I) and Na(I) while about 40% were replaced by Cs(I) with an overall molar ratio of 1:15:34:47:69 = Li/Na/K/Rb/Cs.

Photoluminescence was found to occur under excitation at 340 nm showing a broad band around 470 nm in solid-state emission; the group attributes this to intra-ligand electron state transitions. Ion exchange with metal cations doesn't produce significant change in the emission band but rather the intensity and quantum yield are affected depending on the metal. Potassium and rubidium produced the most pronounced effect with around a 30% reduction, with cesium at a 19% reduction.

3.9.4   Metal-organic framework-based ion traps for irreversible barium adsorption [43]

Yagyuang Peng, Hongliang Huang, et al. had work published in Applied Materials & Interfaces by ACS in 2016 regarding a zirconium-based MOF (MOF-808-SO_4, or Zr-MOF) postsynthetically functionalized with sulfate groups, as well as a chromium-based MOF (MIL-101-SO_3H, or Cr-MOF) with in situ sulfonic acid functionality for the highly efficient, irreversible uptake of Ba(II). The former exhibits excellent uptake capacity while the latter possesses rapid uptake kinetics.

Both Zr-MOF and Cr-MOF were characterized using PXRD, revealing by comparison to synthesis of unfunctionalized parent materials that both exhibit appropriate crystal structure. The decrease in N_2 adsorption corroborates a decreased BET surface area due to sulfate/sulfonic acid functionalization. The successful amendment of both MOFs with respective sulfur groups was shown by FT-IR and XPS. Sulfur-oxygen stretching bands at 1135 and 1080 wavenumbers, as well as sulfur 2p binding energies of 168.8 and 168.0 eV for Zr-MOF and Cr-MOF, respectively, are attributed to the attachment of the moieties to each framework. These values were found to shift for Zr-MOF with uptake of Ba(II). TGA and ICP reveal no excess Zr or Cr present in the MOF materials. This was done by comparing metal content of theoretical models of Zr-MOF and Cr-MOF with experimental metal content.

Barium uptake studies were performed at an optimized 5.8 pH in aqueous solutions. Both Zr-MOF and Cr-MOF were shown to include >90% of Ba(II) in 5 minutes, and >99% at equilibrium; Cr-MOF showed faster overall sorption. The group attributes this quality to superior pore structure. Cr-MOF induced a decrease in pH to 4.7 while Zr-MOF did not due to differing sorption mechanisms, where the sulfonic group chelates the metal by proton exchange. This mechanism was used to explain Cr-MOF's lower capacity in terms of ion competition. Sorption isotherms were used to show almost no uptake in parent materials, while Zr-MOF possesses a saturation capacity of 131.1 mg g^{-1} and Cr-MOF's is 70.5 mg g^{-1}. Cr-MOF vastly outperforms many sorbents used for this purpose. Adsorption across a temperature range was determined to be an endothermic process by calculation of the adsorption free energy.

Selectivity for Ba(II) was characterized against ions present in nuclear wastewater (Cs(I), Zn(II), Ni(II), Co(II), Sr(II), La(III), Eu(III)) as shown in Fig. 3.18.

Both MOFs maintain an efficiency over 93% in mixed metal ion solutions with concomitant ions having a magnitude higher concentration. Release of Ba(II) into clean water was found to be small. Each MOF was saturated with Ba(II) and rinsed with water, then allowed to soak with shaking for 7 days. Zr-MOF retained 98% while Cr-MOF retained 92% of adsorbed Ba(II)—this was determined by ICP of the MOFs.

The lower uptake capacity for Cr-MOF is believed to be due to its competitive ion mechanism as well as the nature of its functional group. The sulfonic acid is partly less active due to the terephthalate ligand it is attached to, making the lower uptake particularly evident when compared to Zr-MOF, where the sulfate group is connected to the metal cluster and does not experience the competitive ion effect or the deactivation as illustrated in Fig. 3.19. This interpretation is reinforced by DFT calculations [44].
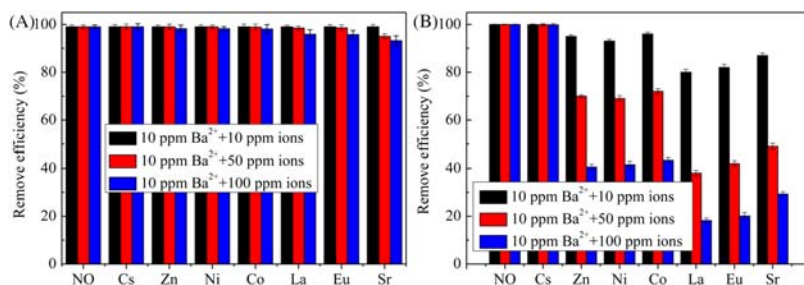
Figure 3.18 Effect of mixed metal ions on the adsorption of Ba(II) by Zr-MOF (A) and Cr-MOF (B).

Source: Adapted from Y. Peng, H. Huang, D. Liu, C. Zhong, Radioactive barium ion trap based on metal-organic framework for efficient and irreversible removal of barium from nuclear wastewater, ACS Appl. Mater. Interfaces 8 (13) (2016) 8527−8535 with permission from the American Chemical Society.
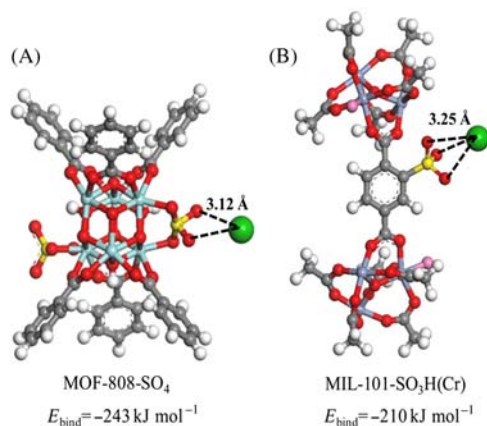
Figure 3.19 Optimized geometries illustrating the interactions of Ba(II) with Zr-MOF metal cluster (A) and Cr-MOF ligand (B) (*Zr in cyan, Cr light blue, Ba green, C gray, S yellow, O red, H white*).
Source: Adapted from Y. Peng, H. Huang, D. Liu, C. Zhong, Radioactive barium ion trap based on metal-organic framework for efficient and irreversible removal of barium from nuclear wastewater, ACS Appl. Mater. Interfaces 8 (13) (2016) 8527−8535 with permission from the American Chemical Society.

3.9.5 Terbium-based metal-organic framework for selective uranium detection [45]

Wei Liu, Xing Dai, et al. had work published in Environmental Science & Technology in 2017 regarding a terbium MOF (Tb-MOF) functionalized with highly Lewis basic ligands for the selective sensing of uranyl (UO_2^{2+}) in aqueous solutions. Tb-MOF was synthesized under solvothermal conditions and its structure determined by single-crystal X-ray revealing a mesoporous, noninterpenetrated 3D framework. It was found to have a surface area of $525 \, cm^2 \, g^{-1}$ based on the BET method. The H_3TATAB ligands in the material orient such that the extensive Lewis basic amine and triazine sites were coordinated inwards toward the pore voids with carboxylate groups connecting to the $[Tb_2(CO_2)_4]$ metal clusters (Fig. 3.20). Hydrolytic stability was confirmed by aging in various metal salt solutions as well as real lake and seawater samples with pH ranging from 2 to 10. Solubility of Tb-MOF in these solutions was found to be low, ranging from 1.15% to 5.35% lost to solution at pH 4, which was decidedly the optimized pH for uptake. Gamma radiation resistance ensures application to HLW solutions.

Fluorescence detection experiments were carried out by establishing presence of characteristic Tb(III) transition bands at 488, 545, 581, and 620 nm—each representing a 4f-4f transition type [46] with a quantum yield up to 44.8%. Following, Tb-MOF was saturated with various concentrations of $UO_2(NO_3)6(H_2O)$ in deionized water at pH 4. Quenching was attributed to LMCT and supported by DFT calculations, EXAFS, and XANES—it could be observed by the naked eye. The Langmuir model was used to fit the quenching ratio as a function of uranium
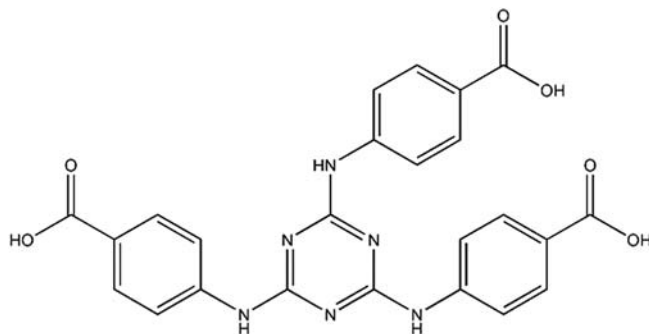
**Figure 3.20** H$_3$TATAB (4,4′,4″-((1,3,5-triazine-2,4,6-triyl)tris(azanediyl))tribenzoic acid). *Source*: Adapted from J. Zhao, Y.-N. Wang, W.-W. Dong, Y.-P. Wu, D.-S. Li, Q.-C. Zhang, A robust luminescent Tb (III)-MOF with Lewis basic pyridyl sites for the highly sensitive detection of metal ions and small molecules, Inorg. Chem. 55 (7) (2016) 3265−3271 with permission from the American Chemical Society.

concentration with an R^2 value of 0.9911. Further, the quotient of uranyl concentration and the quenching ratio as a function of uranyl concentration revealed an impressive R^2 value of 0.9999, suggesting a highly accurate quantitative detection of uranyl over a concentration range of 0.2−350 mg L^{-1}. Adsorption kinetics study showed a reasonably fast uptake with 98% removal at pH 4 at 5 and 50 mg L^{-1}. The LOD was shown to be Tb-MOF concentration dependent and was optimized to 0.05 g L^{-1} of Tb-MOF in uranyl solution. The LOD value under these ideal conditions was determined to be 0.9 μg L^{-1}.

Selectivity was characterized by a battery of highly concentrated (0.5 g L^{-1}) metal nitrate solutions (Th(IV), Eu(III), Al(III), Sr(II), Ca(II), Cs(I), Cs(I), and K(I)) and several mixed solutions of these metal nitrates. In the former, after confirmation of a negligible effect (except for Eu(III)), uranyl was added and found to effectively quench each solution's luminescence. In the latter case, it was found that these mixed metal ion solutions did not prevent selective uranyl uptake by Tb-MOF (Fig. 3.21).

Sorption was further characterized for NaCl, Na$_2$CO$_3$, and humic acid (a component of soil) mixtures. In all cases uranyl uptake remained above 93%. Calculations on tests run with fresh lake and seawaters reported LODs of 14.0 and 3.5 μg L^{-1}, respectively. An artificial seawater sample containing uranium was used to give perspective against ICP-MS determination of uranyl content. This technique reported a concentration of 114.6 μg L^{-1} while the method described in this work reported 106.7 μg L^{-1}.

The pore environment and adsorption mechanism were elucidated by XANES, EXAFS, and DFT calculations. It was found that various degrees of hydrated uranyl are chelated via U-N bonding to the lone pairs of the Lewis basic sites primarily in a hexagonal bipyramid coordination geometry rather than interacting with oxygen of the carboxylate groups, which are saturated by Tb and sterically hindered by hydrophobic benzene. Uranyl complexation in this way has a negative free energy indicating thermodynamic favor.
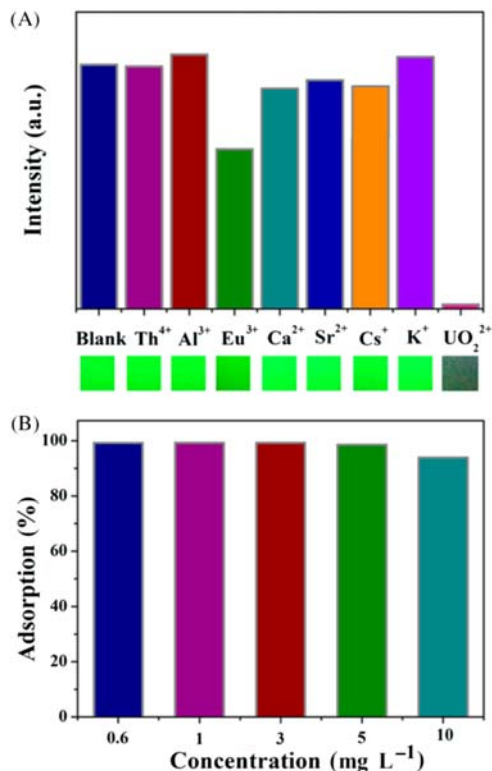
Figure 3.21 (A) Luminescence intensity of Tb-MOF in various metal ion solutions with respective image of luminescence under UV light. (B) Uranyl adsorption ratio in mixed metal ion solutions at various concentrations.
Source: Adapted from J. Zhao, Y.-N. Wang, W.-W. Dong, Y.-P. Wu, D.-S. Li, Q.-C. Zhang, A robust luminescent Tb (III)-MOF with Lewis basic pyridyl sites for the highly sensitive detection of metal ions and small molecules, Inorg. Chem. 55 (7) (2016) 3265−3271 with permission from the American Chemical Society.

References

[1] Y. Georgiou, J.A. Perman, A.B. Bourlinos, Y. Deligiannakis, Highly efficient arsenite [As(III)] adsorption by an [MIL-100(Fe)] metal−organic framework: structural and mechanistic insights, J. Phys. Chem. C 122 (9) (2018) 4859−4869.

[2] E. Tahmasebi, M.Y. Masoomi, Y. Yamini, A. Morsali, Application of mechanosynthe-sized azine-decorated zinc (II) metal−organic frameworks for highly efficient removal and extraction of some heavy-metal ions from aqueous samples: a comparative study, Inorg. Chem. 54 (2) (2014) 425−433.

[3] F. Ke, L.-G. Qiu, Y.-P. Yuan, F.-M. Peng, X. Jiang, A.-J. Xie, et al., Thiol-functionalization of metal-organic framework by a facile coordination-based postsyn-thetic strategy and enhanced removal of Hg^{2+} from water, J. Hazard. Mater. 196 (2011) 36−43.

[4] Z. Hu, B.J. Deibert, J. Li, Luminescent metal−organic frameworks for chemical sensing and explosive detection, Chem. Soc. Rev. 43 (16) (2014) 5815−5840.

[5] W. Morris, W.E. Briley, E. Auyeung, M.D. Cabezas, C.A. Mirkin, Nucleic acid−metal organic framework (MOF) nanoparticle conjugates, J. Am. Chem. Soc. 136 (20) (2014) 7261−7264.

[6] Wolfgang Maret, J-MM. Cadmium: From Toxicity to Essentiality 2013.

[7] T. Nawrot, M. Plusquin, J. Hogervorst, H.A. Roels, H. Celis, L. Thijs, et al., Environmental exposure to cadmium and risk of cancer: a prospective population-based study, Lancet Oncol. 7 (2) (2006) 119−126.

[8] T.S. Nawrot, J.A. Staessen, H.A. Roels, E. Munters, A. Cuypers, T. Richart, et al., Cadmium exposure in the population: from health risks to strategies of prevention, Biometals 23 (5) (2010) 769−782.

[9] M. Nordberg, J. Duffus, D.M. Templeton, Glossary of terms used in toxicokinetics (IUPAC Recommendations 2003), Pure Appl. Chem. (2004) 1033.

[10] H. Xue, Q. Chen, F. Jiang, D. Yuan, G. Lv, L. Liang, et al., A regenerative metal-organic framework for reversible uptake of Cd(ii): from effective adsorption to in situ detection, Chem. Sci. 7 (9) (2016) 5983−5988.

[11] K.K. Yee, N. Reimer, J. Liu, S.Y. Cheng, S.M. Yiu, J. Weber, et al., Effective mercury sorption by thiol-laced metal-organic frameworks: in strong acid and the vapor phase, J. Am. Chem. Soc. 135 (21) (2013) 7795−7798.

[12] Y. Wang, G. Ye, H. Chen, X. Hu, Z. Niu, S. Ma, Functionalized metal-organic framework as a new platform for efficient and selective removal of cadmium(ii) from aqueous solution, J. Mater. Chem. A. 3 (29) (2015) 15292−15298.

[13] Y.S. Ho, G. McKay, Pseudo-second order model for sorption processes, Process Biochem. 34 (5) (1999) 451−465.

[14] I. Langmuir, The adsorption of gases on plane surfaces of glass, mica and platinum, J. Am. Chem.Soc. 40 (9) (1918) 1361−1403.

[15] Z. Luo, China's Imperial Tombs and Mausoleums, 1993.

[16] J. Kotaś, Z. Stasicka, Chromium occurrence in the environment and methods of its speciation, Environ. Pollut. 107 (3) (2000) 263−283.

[17] D.C. Schroeder, G.F. Lee, Potential transformations of chromium in natural waters, Water, Air, Soil Pollution 4 (3) (1975) 355−365.

[18] K.G. Stollenwerk, D.B. Grove, Adsorption and desorption of hexavalent chromium in an alluvial aquifer Near Telluride, Colorado1, J. Environ. Qual. 14 (1) (1985) 150−155.

[19] H.-R. Fu, Y. Zhao, Z. Zhou, X.-G. Yang, L.-F. Ma, Neutral ligand TIPA-based two 2D metal-organic frameworks: ultrahigh selectivity of C_2H_2/CH_4 and efficient sensing and sorption of Cr(vi), Dalton Transact. 47 (11) (2018) 3725−3732.

[20] S. Rapti, D. Sarma, S.A. Diamantis, E. Skliri, G.S. Armatas, A.C. Tsipis, et al., All in one porous material: exceptional sorption and selective sensing of hexavalent chromium by using a Zr^{4+} MOF, J. Mater. Chem. A. 5 (28) (2017) 14707−14719.

[21] T.-F. Liu, D. Feng, Y.-P. Chen, L. Zou, M. Bosch, S. Yuan, et al., Topology-guided design and syntheses of highly stable mesoporous porphyrinic zirconium metal-organic frameworks with high surface area, J. Am. Chem. Soc 137 (1) (2015) 413−419.

[22] D. Sun, Y. Fu, W. Liu, L. Ye, D. Wang, L. Yang, et al., Studies on photocatalytic CO_2 reduction over NH_2-Uio-66(Zr) and its derivatives: towards a better understanding of photocatalysis on metal−organic frameworks, Chem. Europ. J. 19 (42) (2013) 14279−14285.

[23] J.O. Nriagu, Saturnine gout among roman aristocrats, New Engl. J. Med. 308 (11) (1983) 660−663.

[24] A. Torrago, Case studies in environmental medicine (CSEM) lead toxicity, Agency Toxic Subst. Disease Registry (2012).

[25] D.C. Baxter, W. Frech, Speciation of lead in environmental and biological samples (Technical Report), Pure Appl. Chem. (1995) 615.

[26] S. Sauvé, M.B. McBride, W.H. Hendershot, Speciation of lead in contaminated soils, Environ. Pollut. 98 (2) (1997) 149−155.

[27] G. Ji, J. Liu, X. Gao, W. Sun, J. Wang, S. Zhao, et al., A luminescent lanthanide MOF for selectively and ultra-high sensitively detecting Pb^{2+} ions in aqueous solution, J. Mater. Chem. A 5 (21) (2017) 10200−10205.

[28] J.-N. Hao, B. Yan, A water-stable lanthanide-functionalized MOF as a highly selective and sensitive fluorescent probe for Cd_{2+}, Chem. Commun. 51 (36) (2015) 7737−7740.

[29] L. Cui, J. Wu, J. Li, H. Ju, Electrochemical sensor for lead cation sensitized with a DNA functionalized porphyrinic metal−organic framework, Anal. Chem. 87 (20) (2015) 10635−10641.

[30] E.Y. Park, Z. Hasan, I. Ahmed, S.H. Jhung, Preparation of a composite of sulfated zirconia/metal organic framework and its application in esterification reaction, Bullet. Korean Chem. Soc. 35 (6) (2014) 1659−1664.

[31] M.A. Atwood, A Suggestive Inquiry Into the Hermetic Mystery: With a Dissertation on the More Celebrated of the Alchemical Philosophers Being an Attempt Towards the Recovery of the Ancient Experiment of Nature 19, Kessinger Publishing, 1999.

[32] J.G. Omichinski, Toward methylmercury bioremediation, Science 317 (5835) (2007) 205.

[33] K.M. Rice, E.M. Walker, M. Wu, C. Gillette, E.R. Blough, Environmental mercury and its toxic effects, J. Prev. Med. Public Health 47 (2) (2014) 74−83.

[34] L. Sa, W. Stratton, Atmospheric mercury speciation: concentrations and behavior of reactive gaseous mercury in ambient air, Environ. Sci. Technol. 32 (1) (1998) 49−57.

[35] X. Zhang, T. Xia, K. Jiang, Y. Cui, Y. Yang, G. Qian, Highly sensitive and selective detection of mercury (II) based on a zirconium metal-organic framework in aqueous media, J. Solid State Chem. 253 (2017) 277−281.

[36] V. Guillerm, S. Gross, C. Serre, T. Devic, M. Bauer, G. Ferey, A zirconium methacrylate oxocluster as precursor for the low-temperature synthesis of porous zirconium(iv) dicarboxylates, Chem. Commun. 46 (5) (2010) 767−769.

[37] L.L. Wu, Z. Wang, S.N. Zhao, X. Meng, X.Z. Song, J. Feng, et al., A metal−organic framework/DNA hybrid system as a novel fluorescent biosensor for mercury(II) ion detection, Chem. Europ. J. 22 (2) (2016) 477−480.

[38] H. Urata, E. Yamaguchi, T. Funai, Y. Matsumura, W. Si, Incorporation of thymine nucleotides by DNA polymerases through T−HgII−T base pairing, Angew. Chem. 122 (37) (2010) 6666−6669.

[39] S. Halder, J. Mondal, J. Ortega-Castro, A. Frontera, P. Roy, A Ni-based MOF for selective detection and removal of Hg^{2+} in aqueous medium: a facile strategy, Dalton Transact. 46 (6) (2017) 1943−1950.

[40] P.D. Wilson, The Nuclear Fuel Cycle from Ore to Wastes, Oxford University Press, 1996.

[41] Radiation UNSCotEoA, Sources and Effects of Ionizing Radiation, United Nations Publications, 2000.

[42] S.A. Sapchenko, P.A. Demakov, D.G. Samsonenko, D.N. Dybtsev, M. Schröder, V.P. Fedin, A cryptand metal−organic framework as a platform for the selective uptake and detection of group I metal cations, Chem. Europ. J. 23 (10) (2017) 2286−2289.

[43] Y. Peng, H. Huang, D. Liu, C. Zhong, Radioactive barium ion trap based on metal−organic framework for efficient and irreversible removal of barium from nuclear wastewater, ACS Appl. Mater. Interfaces 8 (13) (2016) 8527−8535.
[44] M. Frisch, G. Trucks, H. Schlegel, G. Scuseria, M. Robb, J. Cheeseman, et al., Gaussian 03, Revision c. 02, Gaussian Inc, Wallingford, CT, 2004, p. 4.
[45] J. Zhao, Y.-N. Wang, W.-W. Dong, Y.-P. Wu, D.-S. Li, Q.-C. Zhang, A robust luminescent Tb (III)-MOF with Lewis basic pyridyl sites for the highly sensitive detection of metal ions and small molecules, Inorg. Chem. 55 (7) (2016) 3265−3271.
[46] W. Liu, X. Dai, Z. Bai, Y. Wang, Z. Yang, L. Zhang, et al., Highly sensitive and selective uranium detection in natural water systems using a luminescent mesoporous metal−organic framework equipped with abundant lewis basic sites: a combined batch, X-ray absorption spectroscopy, and first principles simulation investigation, Environ. Sci. Technol. 51 (7) (2017) 3911−3921.